Organic Electronics 26 (2015) 48–54

Contents lists available at ScienceDirect

Organic Electronics

journal homepage: www.elsevier.com/locate/orgel

Morphology construction of vertical phase separation for large-area polymer solar cells

Fan Wu [a,b,c], Feng Ye [a,b,c], Zhaobin Chen [a,b], Yi Cui [a,b], Dalei Yang [a,b,c], Zidong Li [a,b,c], Xiaoli Zhao [a,b,*], Xiaoniu Yang [a,b,*]

[a] Polymer Composites Engineering Laboratory, Changchun Institute of Applied Chemistry, Chinese Academy of Sciences, 5625 Renmin Street, Changchun 130022, PR China
[b] State Key Laboratory of Polymer Physics and Chemistry, Changchun Institute of Applied Chemistry, Chinese Academy of Sciences, 5625 Renmin Street, Changchun 130022, PR China
[c] University of Chinese Academy of Sciences, Beijing 100049, PR China

ARTICLE INFO

Article history:
Received 14 April 2015
Received in revised form 29 June 2015
Accepted 5 July 2015
Available online 13 July 2015

Keywords:
Polymer solar cells
Large-area
X-ray photoelectron spectroscopy
Vertical phase separation
Ultrasonic spray

ABSTRACT

Although the power conversion efficiency (PCE) of small-area polymer solar cells (PSCs) has now surpassed 10% upon various optimizations, it is still a challenge to improve the performance of large-area device partially due to the problems encountered in film morphology optimization and incompatibility of using these optimizations for size scale-up. Herein, we reported a method to effectively improve the morphology of photoactive layer and thus device efficiency under ambient atmosphere by using spray coating technique. It was found that by finely adjusting the parameters of the instrument, and the properties of the "electronic ink", the dynamics of solvent evaporation after film deposition could be controlled. By resorting to a few techniques for morphology characterization, it confirmed that the resulting blend film showed desirable vertical phase separation where polymer enriched near the anode and PCBM adjacent to the cathode. The graded composition is beneficial for the efficient charge transportation as well as eventual charge collection. By using PBDT-TFQ/$PC_{71}BM$ composite as an example, the exceptional high PCEs of 4.6% and 4.1% were achieved for the devices with the size of 1.0 and 10.2 cm^2, respectively. In comparison to conventional device fabrication process, this method is not only simple without additional treatment steps, but also dramatically increases the device efficiency, which opens a new way for fabricating highly efficient large-area PSCs.

1. Introduction

Polymer solar cells (PSCs) have drawn significant attention owing to their outstanding advantages of light weight with flexibility, solution processability through various techniques, and low-cost production over large area [1,2]. Due to high reproducibility and precision [3], the spin coating technique is the most used method for fabrication of small-area device (typically few square millimeters), and much effort has been devoted to the optimization of fabrication conditions [4,5], development of post-treatment methods [6–10], and synthesis of new conjugated polymers [11–13]. To date, the power conversion efficiency (PCE) of small-area PSC devices has reached over 10% threshold [14,15].

It is well recognized that besides the synthesis of new conjugated polymers, the morphology of the active layer plays the most important role in determining the device PCE [7,16]. Therefore, different post-treatment methods, such as thermal annealing [6,7], solvent annealing [8], and processing additives [9,10], etc., have been created allowing further enhancement in PCE. In general, the optimization of the film morphology should be started from both lateral and vertical directions, and the vertical morphology is of utmost importance because the charge carriers transport to corresponding electrodes along this direction [17–20]. Unfortunately, most of the methods focus on former aspect, and although solvent vapor annealing [21], solvent-soaking treatment [22], and methanol-fluxing treatment [17,23] were recently developed to tailor the vertical phase morphology, these methods are directed to the spin-coated small-area polymer solar cells.

The ultimate goal of the research in polymer solar cells is to scale-up the size of the device to fabricate modules in real applications. Until now, various techniques, such as inkjet printing [24,25], slot-die coating [26,27], screen printing [28–30], doctor blading [31], gravure printing [32–34], and spray coating [19,35–48], have been developed to prepare the large-area polymer solar cells, and promising efficiencies have been obtained

* Corresponding authors at: Polymer Composites Engineering Laboratory, Changchun Institute of Applied Chemistry, Chinese Academy of Sciences, 5625 Renmin Street, Changchun 130022, PR China.
E-mail addresses: zhaoxiaoli@ciac.ac.cn (X. Zhao), xnyang@ciac.ac.cn (X. Yang).

http://dx.doi.org/10.1016/j.orgel.2015.07.010
1566-1199/

for each technique. However, in comparison to small-area device, the low homogeneity of the blend film and the thus resulting defects (such as disconnected and short-circuited areas) during large-scaling process heavily limit the module's PCE promotion [49,50]. Although the treatment methods mentioned above could improve the film morphology to some extent, the difference in efficiencies between small and large size devices still could not be made up. In addition, these current post-treatment methods are also not applicable for large-area polymer solar cells due to energy consuming, operation complexity, and environmental concerns.

For the fabrication of large-area polymer solar cells, the morphology control is much more complicated because it depends not only on the instrument type but also on the operation parameters [51–53]. Our experience on flexible and scalable polymer solar cells in the last few years shows that it is possible to precisely regulate the morphology of the active layer (especially along the vertical direction) by selecting appropriate instrument and finely adjusting the operation parameters, and thus greatly increase the PCE [54]. To demonstrate this strategy, in this study, the ultrasonic spray coating technique was utilized, and the "electronic ink" composed of poly{4,8-bis(2′-ethylhexyloxy)-benzo[1,2-b:4,5-b′]-dithiophene-alt-[5,8-bis(5′-thiophen-2′-yl)-6,7-difluoro-2,3-bis-(3″-hexyloxyphenyl)quinoxaline]} (PBDT-TFQ) [55] as electron donor and [6,6]-phenyl-C_{71}-butyric acid methyl ester ($PC_{71}BM$) as electron acceptor was selected to prepare the active layer. After precise adjustment of the operation conditions (especially the ink flow rate and the number of spray passes) and the properties of the solution (with and without processing additive), it was found that the active layer with desired vertical component distribution could be obtained while the lateral phase structure was kept unchanged. The efficiency of the large-area devices with the size of 1.0 and 10.2 cm^2 based on this technique reaches as high as 4.6% and 4.1%, respectively. This method, the principle of which could be applicable for other techniques, is simple, cost-effective, and easy to operate with no need of any post-treatment steps, and shows great potentials in the fabrication of large-area polymer solar cells.

2. Experimental section

2.1. Materials

PBDT-TFQ (M_n = 35 kg mol^{-1}, PDI = 2.0) was prepared according to the previous literature [55]. $PC_{71}BM$, 1,8-diiodooctane (DIO) and chlorobenzene (CB, anhydrous, 99%) were purchased from Sigma–Aldrich. PEDOT:PSS (Clevios P VP AI 4083) was purchased from H.C. Stark company.

2.2. Spray coater

Ultrasonic spray coating systems (ExactaCoat W4301) was purchased from Sono-Teck Corporation (Fig. 1). For spraying, the ink is pumped to the nozzle at a settled flow rate and broken into micro scale droplets by the ultrasonic vibration, and then the droplets are directed toward the substrates by the carrier gas. In the process, the variety of parameters including carrier gas pressure, nozzle scan speed, ultrasonic power, nozzle to substrates distance, flow rate of the ink and the number of spray passes over the substrate can be manipulated. The carrier gas pressure can vary from 0 to 23.4 psi. The maximum nozzle scan speed is 200 mm s^{-1}. The maximum ultrasonic power is 5.5 watt. The nozzle to substrates distance can vary from 6 to 12 cm. Flow rate depends on the capacity of the syringe used and the speed at which the syringe plunger is moved forward. For the 10 ml syringe that is used in our experiment, the maximum flow rate is 20.9 ml min^{-1}. For the

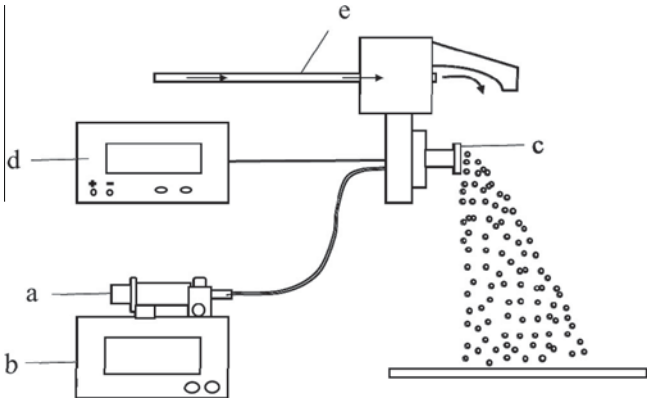

Fig. 1. Schematic diagram of spray-coater. (a) Syringe, (b) auto-solution injection pump: controlling the injected flow rate of the ink, (c) ultrasonic nozzle: atomizing the ink into droplet, (d) ultrasonic generator: supplying power and controlling frequency of the nozzle, (e) carrier gas controller: controlling gas pressure to deposit solution onto the substrate.

films in the following discussion, the parameters including carrier gas pressure, nozzle scan speed, ultrasonic power, and distance between nozzle and substrates are fixed at 23.4 psi, 30 mm s^{-1}, 3.5 watt, and 6 cm, respectively. And, the flow rate of the electronic ink and the number of spray passes are varied from 0.12 to 0.35 ml min^{-1} and 2 to 6, respectively. Correspondingly, the films are named as Film LH, Film MM and Film HL (Table 1), of which the former letter represents the flow rate and the latter letter represents the number of spray passes. L, M, and H represent low, medium and high values of the corresponding spray parameters, respectively. For example, Film LH means the film is deposited under the low flow rate of 0.12 ml min^{-1} and the high number of spray passes of 6.

2.3. Device fabrication

The organic ink was prepared by dissolving PBDT-TFQ:$PC_{71}BM$ (1:1, w/w) in a mixture of 1,8-diiodooctane (2 vol%) and chlorobenzene (98 vol%), the total solid concentration is 4 mg ml^{-1}. The PEDOT:PSS ink was prepared by diluting PEDOT:PSS with deionized water and isopropanol in the ratio of 18:9:73 by volume [42,56].

The PSCs were prepared on pre-patterned ITO-coated glass with a sheet resistance of *ca.* 15 Ω per square. The ITO substrates were cleaned sequentially in detergent, deionized water and isopropanol. After UV ozone treatment for 30 min, a *ca.* 30 nm PEDOT:PSS layer was spray deposited onto the substrate and annealed at 150 °C for 20 min to remove the residual solvent and enhance the conductivity. The photoactive layers with a thickness of *ca.* 120 nm were spray deposited onto the PEDOT:PSS layer from the organic ink in air and then thermal annealed at 140 °C for

Table 1
Blend film spray parameters.*

	Flow rate (ml min^{-1})	Number of spray passes
Film LH	0.12	6
Film MM	0.17	4
Film HL	0.35	2

* *Note*:(a) Sample solution is PBDT-TFQ and $PC_{71}BM$ (1:1, weight ratio) in a solvent mixture of 1,8-diiodooctane (DIO, 2 vol%) and chlorobenzene (CB, 98 vol%), the total solid concentration is 4 mg ml^{-1}.(b) Other parameters: carrier gas pressure is 23.4 psi, nozzle scan speed is 30 mm s^{-1}, ultrasonic power is 3.5 watt, distance between nozzle and substrates is 6 cm.

10 min in a nitrogen glove box with the concentration of H_2O < 0.1 ppm and of O_2 < 1.0 ppm.

Finally, Ca/Al (30 nm/100 nm) layer was thermally evaporated on the photoactive layer through shadow masks. The active area of each device was defined by overlap of the metal electrode and ITO. The devices with areas of 9 mm^2 (3 mm × 3 mm), 1.0 cm^2 (10 mm × 10 mm), 10.2 cm^2 (12 mm × 85 mm) were obtained with the changing ITO patterns and shadow masks. Devices based on Film LH, Film MM and Film HL were named as Device LH, Device MM and Device HL, respectively.

The device performance was measured in a nitrogen glove box with the concentration of H_2O < 0.1 ppm and of O_2 < 1.0 ppm with a Keithley 2400 source meter under an AM 1.5G solar simulator (SAN-EI, XES-70S1 (AAA Class Standard)).

2.4. Measurement

UV–Vis absorption spectra were taken on a Lambda 750 spectrometer (Perkin-Elmer, Wellesley, MA).

X-ray Diffraction (XRD) measurements were performed on a Rigaku Smart Lab X-ray diffractometer with X-ray generation power of 44 kV tube voltage and 40 mA tube current. The diffraction was acquired at θ-2θ symmetry within the range of 2θ = 3–15°.

Transmission electron microscope (TEM) images were acquired with a JEOL JEM-1011 transmission electron microscope operated at an acceleration voltage of 100 kV. The samples for TEM experiments were obtained by floating thin films on water and then transferring them onto copper grids.

X-ray photoelectron spectroscopy (XPS) measurements were carried out on VG ESCALAB MK II X-ray photoelectron spectroscope and the probing depth was less than 10 nm. The blend films were lifted off from the substrates by deionized water, and then transferred to new conductive substrates with the selected face on the top for XPS measurement. Specifically, the films were kept in water at 50–60 °C for 10 min before transferring to new substrates in order to remove PEDOT:PSS which was well dissolved in water.

Surface tension and contact angle measurement were performed on an optical contact angle measuring device (KRUSS, DSA30). The solutions of $PC_{71}BM$/DIO, PBDT-TFQ/CB, and $PC_{71}BM$/CB were dissolved at a concentration of 2 mg ml^{-1}. The surface tensions of the solutions were measured by the pendant drop method [56]. The contact angle of the solutions were carried out on spin-coated PEDOT:PSS surfaces. The surface characterization was carried out on an A1m polarization microscope (Carl Zeiss, Germany). The film thickness was measured with a KLA Tencor D100 stylus profilometer.

3. Results and discussion

3.1. Preparation and characterization of photoactive layer

The spray-coater employed in this work was purchased from Sono-Teck Corporation (Exactacoat W4301), its schematic diagram is shown in Fig. 1. The operation principle of the instrument is that the solution ink in the syringe (a) is first pumped (b) into the ultrasonic nozzle (c), which is then broken into micro scale droplets by ultrasonic vibration (d), and the droplets are finally deposited onto the substrate surface by carrier gas (e) to form the blend film. During this process, the quality of the formed blend film depends on many factors, for example, the properties of the "electronic ink" (organic solvent, concentration, and processing additive), and the operation parameters, including carrier gas pressure, ultrasonic generator power, nozzle scan speed, distance between nozzle and substrate, flow rate of the ink, and the number of spray passes over the substrate. These factors are interconnected and influence each other.

As mentioned above, the parameters of the spray coater could be adjusted in a wide range and could be divided into three regimes: wet, intermediate, and dry according to the different solvent evaporation rate after liquid droplets leaving nozzle. In wet regime, the deposited droplets merge into discrete and larger droplets due to the dewetting effect before the complete evaporation of solvent, resulting in a "wet" and extremely uneven film. In dry regime, solvents evaporate completely before the droplets reach the substrate and solutes in the droplet become a dust, which leads to a "dry" and quite rough film (Fig. S1). For spray coating technique, the intermediate regime which lies between the wet and dry regimes is most appropriate because a smooth and continuous film with homogeneous morphology could be formed. And, we defined this uniform film as the "half-wet" (or "half-dry") film. Since the operation parameters of the spray coater affect each other, in this study, the flow rate of the electronic ink and the number of spray passes are the two main parameters that are finely adjusted to construct the precisely designed vertical phase structure while the other parameters are kept unchanged (Table 1). Under the conditions listed in Table 1, the freshly deposited films on the substrate are "half-wet", while the solvent evaporation is different after the film deposition.

The properties of PBDT-TFQ/$PC_{71}BM$ blend film were first characterized by UV–Vis and XRD analyses, and the corresponding spectra are given in Fig. S2. For conjugated PBDT-TFQ polymer, the peak at 620 nm in UV–Vis spectrum and the peak at 2θ = 4.16° in XRD curve are assigned to the stacking of the molecular chains and (100) crystal planes, respectively [55]. The comparison of these data (Fig. S2 and Table S1) shows that the spray parameters used in this study did not bring effects on the ordering and the crystallinity of PBDT-TFQ/$PC_{71}BM$ blend film. TEM observations (Fig. S3), which show bright short PBDT-TFQ nanocrystallines distributed in the whole blend film with no discernable difference, also indicate that the lateral morphology of the blend film is irrespective of the spray parameters.

However, the variation in the flow rate and the number of spray passes do change the vertical component distribution of the blend film, which could be detected by XPS measurement. The XPS profiles of the top (air/photoactive layer) and bottom (photoactive layer/PEDOT:PSS layer) surfaces of PBDT-TFQ/$PC_{71}BM$ blend films and corresponding calculated S/C element ratio are given in Fig. S4 and Table S2, respectively, and the histogram representing the element amount on both surfaces is shown in Fig. 2. For XPS analysis, the C 1s peak stands for the total content of the PBDT-TFQ and $PC_{71}BM$, while S 2p peak comes only from the PBDT-TFQ component. From Fig. 2 it can be seen that as the number of spray passes increases (the flow rate decreases) from twice

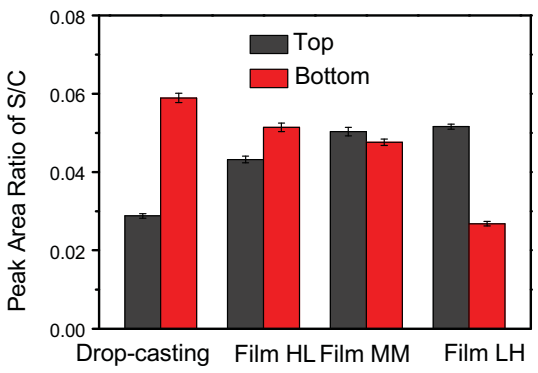

Fig. 2. Histogram of the S/C element ratio at top and bottom surfaces.

Table 2
Surface properties of $PC_{71}BM$/DIO, PBDT-TFQ/CB, and $PC_{71}BM$/CB solutions.

	Surface tension, γ_L (mN m^{-1})	Contact angle, θ (°) (On PEDOT:PSS)	Spreading parameter, ΔW (mN m^{-1}), (on PEDOT:PSS)
$PC_{71}BM$/DIO	40.6	11.5	−0.81
PBDT-TFQ/CB	27.9	8.3	−0.29
$PC_{71}BM$/CB	27.3	6.0	−0.15

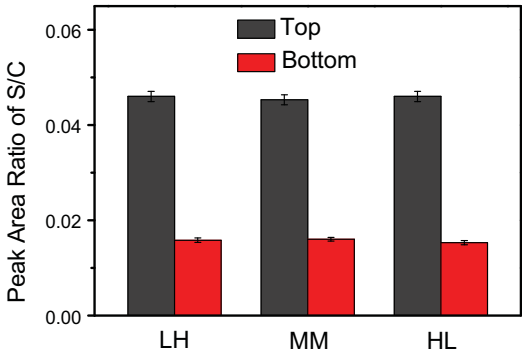

Fig. 3. S/C element ratio of blend films sprayed from solutions without DIO under the parameters of Film LH, MM and HL.

(Film HL) to six times (Film LH), the S/C element ratio on the top surface increases from 0.0432 ± 0.0013 to 0.0516 ± 0.0015, and that on the bottom surface correspondingly decreases from 0.0514 ± 0.0015 to 0.0268 ± 0.0008, indicating the respective enrichment of PBDT-TFQ and $PC_{71}BM$ components on the surfaces of the cathode and anode.

3.2. Formation of vertical phase separation in photoactive layer

Because the other conditions are same except for the flow rate and the number of spray passes during the film preparation, while these two parameters are closely related to the solvent evaporation, therefore, it is reasonable to suggest that the vertical phase structure of the blend film is associated with the solvent evaporation.

This suggestion is demonstrated by the XPS analysis of the drop-casted PBDT-TFQ/$PC_{71}BM$ blend film, the corresponding results are also given in Fig. 2 and Table S2 for reference. In comparison with the spray coated film, the drop-casted film was formed by free standing at room temperature after solution dropping with no additional gas flow, so the solvent evaporation is relatively slower, which results in much lower and higher S/C element ratios (0.0288 ± 0.0009 and 0.0589 ± 0.0018) on top and bottom surfaces and thus the enrichment of the $PC_{71}BM$ and PBDT-TFQ components on respective surfaces.

The formation of the vertical component distribution is also associated with the surface property of solution, the interaction with PEDOT:PSS, and the processing additive (here 1,8-diiodooctane, DIO). The surface tensions (γ_L), contact angles (θ) on PEDOT:PSS layer, and the corresponding spreading parameters (ΔW) of $PC_{71}BM$/DIO, PBDT-TFQ/chlorobenzene (CB), and $PC_{71}BM$/CB solutions are listed in Table 2. The surface tension and the contact angle are measured, while the spreading parameter is calculated from the equation of $\Delta W = \gamma_L(\cos\theta - 1)$, which represents the ability of a liquid drop to adhere to the substrate surface [57]. A more negative spreading parameter indicates less wettability of solution on the solid substrate. As shown in Table 2, the spreading parameter of $PC_{71}BM$/CB (−0.15 mN m^{-1}) is higher than that of PBDT-TFQ/CB (−0.29 mN m^{-1}), indicating the better wettability of $PC_{71}BM$/CB solution on PEDOT:PSS surface. In the presence of the processing additive DIO, which is a better solvent for $PC_{71}BM$ (>120 mg mL^{-1}) and possesses higher boiling temperature (333 °C) relative to the main solvent CB (80 mg mL^{-1}, 132 °C), the surface property of the sample solution are greatly changed. For example, the surface tension and the spreading parameter of the solution with DIO increases to 40.6 mN m^{-1} and decreases to −0.81 mN m^{-1}, respectively, indicating the worse wettability of the solution on PEDOT:PSS surface.

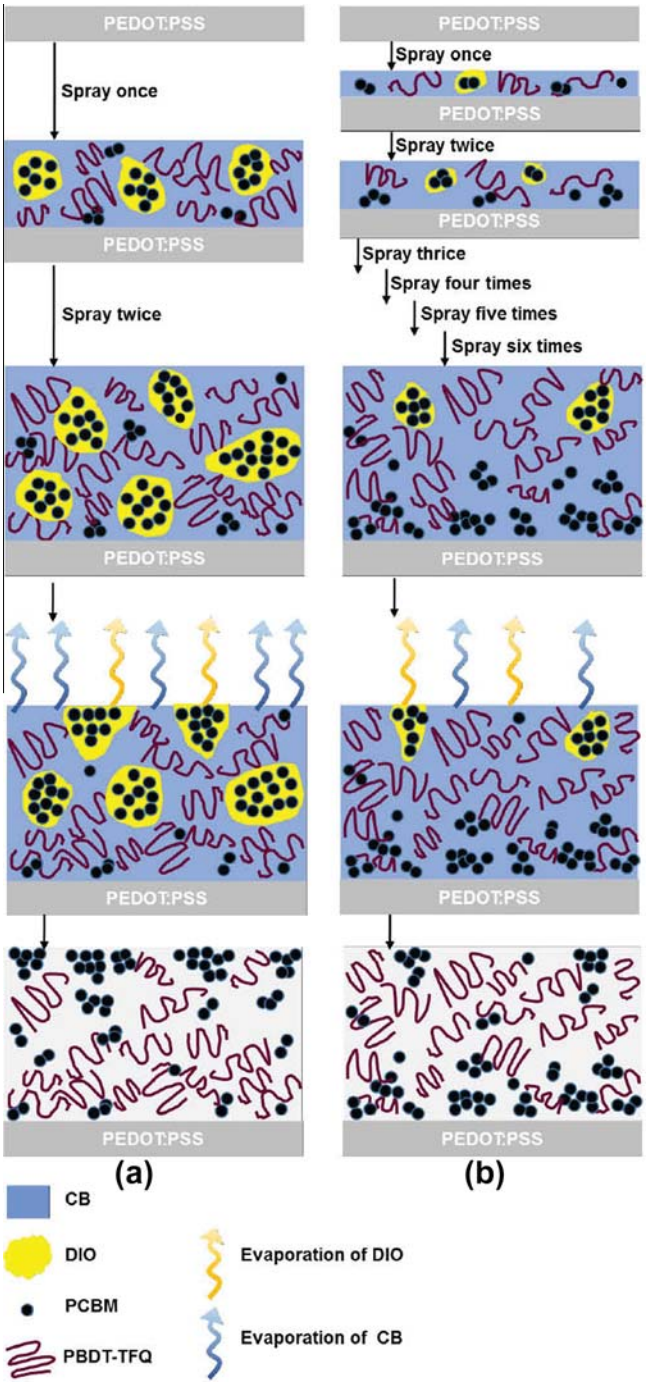

Fig. 4. Schematic of vertical phase separation processes for blend films deposited under different spray-operating parameters (a) Film HL and (b) Film LH.

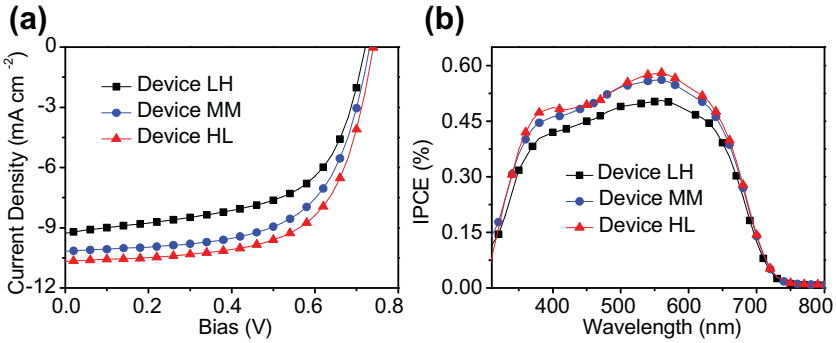

Fig. 5. (a) *J–V* characteristics and (b) IPCE of 9 mm^2 devices based on Film LH, MM, and HL.

Table 3
Performance of 9 mm^2 devices based on Film LH, MM, and HL.

	J_{sc} (mA cm^{-2})	V_{oc} (V)	FF	PCE (%)	Average PCE[a] (%)
Device LH	9.27	0.72	0.59	4.0	3.8
Device MM	10.17	0.74	0.62	4.6	4.5
Device HL	10.67	0.74	0.64	5.1	4.9

[a] Average PCE of 30 devices.

The importance of the processing additive DIO in the construction of the vertical phase separation is verified by XPS analyzing the composition at the top and bottom surfaces of the blend films sprayed from the solution without DIO. The XPS profiles and data are given in Fig. S5 and Table S3. The histogram shown in Fig. 3 reveals that the S/C ratios for the top and bottom surfaces of the three films were around 0.0453 ± 0.0014 and 0.0158 ± 0.0005, respectively, indicating that the desired component distribution along the vertical direction was not constructed for the solution without DIO, even the flow rate and the number of spray passes were finely adjusted for these three blend films (the device performances based on these films were also same, as shown in Fig. S6 and Table S4).

Based on above discussions, the formation of the vertical phase separation of the blend film under different spray conditions is elucidated in terms of the solvent evaporation, surface property, and the diffusion effect, and the schematic is proposed in Fig. 4. For spray coating technique, the formation of the blend film could be divided into two stages: the first stage is the spraying of the solution from the ultrasonic nozzle and moving to the substrate surface, the second stage is the evaporation of the solvent in the half-wet deposited film and the formation of the final solidified blend film. In this study, the solution properties, carrier gas pressure, nozzle scan speed, ultrasonic power, and the distance between nozzle and substrate are kept unchanged except for the flow rate and the number of spray passes, so the size of the droplet, which is determined by the ultrasonic power and solution properties (solvent, concentration), and the solvent evaporation kinetic, which is governed by the carrier gas and the droplet navigating pathway, are same in the first stage for these three films.

The construction process of the vertical phase separation is proposed to occur in the second stage. In order to obtain the blend films with the same thickness, if the flow rate increases from 0.12 ml min^{-1} (Film LH) to 0.35 ml min^{-1} (Film HL), the number of spray passes decreases correspondingly from 6 to 2. For high flow rate (Film HL), as shown in Fig. 4a, the amount of the solution for one time spraying is more and the freshly deposited film in stage two is thicker. In this situation, the surface area/volume ratio is lower and the solvent evaporation is slower. In other words, the amount of the residual solvent in the half-wet deposited blend film is relatively higher. Because DIO has a better solubility for $PC_{71}BM$ in comparison to CB (120 vs. 80 mg ml^{-1}), in this film, the DIO prefers to grasp more $PC_{71}BM$ to form "$PC_{71}BM$/DIO micro-droplet" [58,59]. Since the $PC_{71}BM$/DIO droplet has higher surface tension (40.6 mN m^{-1}) and lower spreading parameter (−0.81 mN m^{-1}), it repels aggregation at the PEDOT:PSS surface. Therefore, the "$PC_{71}BM$/DIO micro-droplet" gradually diffuses to the top surface during the film solidification in the second stage, which finally forms the blend film with the $PC_{71}BM$ component enrichment at the top surface.

In the case of Film LH (Fig. 4b), the flow rate is lower and the number of spray passes is multiple. As mentioned above, the amount of the solution for spraying once is less and the surface/volume ratio is higher for the deposited film at the substrate surface, so the solvent evaporation is rapid. In addition, solvent evaporation is also accelerated by the multiple blowing of the carrier gas. These two effects result in "relatively dry" blend film and the $PC_{71}BM$ is difficult to diffuse to the surfaces. In other words, for

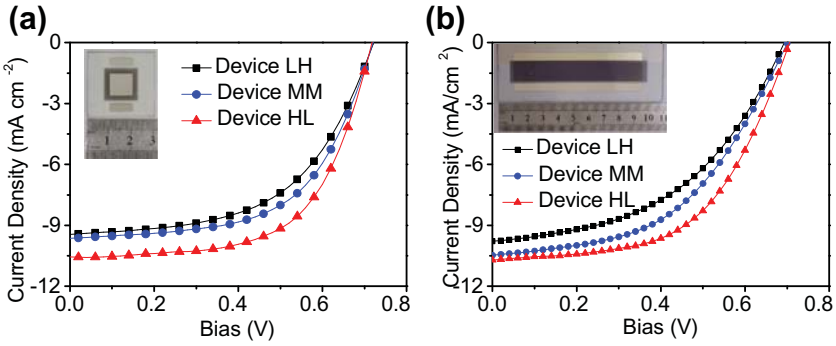

Fig. 6. *J–V* characteristics of (a) 1.0 cm^2 and (b) 10.2 cm^2 devices based on PBDT-TFQ/$PC_{71}BM$ blend films prepared under different spray-operating parameters.

low flow rate and multiple spraying, the time for the complete removal of the solvent is short and the component distribution is rapidly fixed. Therefore, in comparison to Film HL with the vertical phase separation in which $PC_{71}BM$ accumulates on the top surface and PBDT-TFQ enriches on the bottom surface, Film LH shows relatively "homogeneous" morphology along the vertical direction.

3.3. Application of this method for large-area polymer solar cells

In order to explore the effect of the vertical phase separation on device performance, small-area devices (9 mm^2) based on Film LH, MM and HL were fabricated. The *J–V* characteristics and monochromatic incident photo-to-electron conversion efficiency (IPCE) curves of the devices were shown in Fig. 5 (the error between the calculated J_{sc} values and the measurements was within 6%) and the corresponding photovoltaic performances were listed in Table 3. It was found that the formation of the desired vertical phase separation is beneficial for the device performance improvement, the PCE increases from 4.0% of Device LH to 5.1% of Device HL. Detailed insight into the device parameters indicates that the performance improvement is mainly resulted from the increase in short-circuit current and the fill factor. As known, for a PSC with conventional structure, holes and electrons transported towards the anode and cathode through the pathway formed by donor and acceptor material, respectively, and are eventual collected by respective electrodes. So, the desired vertical phase separation in Film HL promotes the efficient charge transportation via the interconnected pathway as well as eventual charge collection at the interface, which contributes to the enhanced J_{sc} and FF, and thus the device efficiency.

This strategy for spray coating technique to control the vertical phase separation of the blend film and thus improve the device performance could also be applied for the fabrication process of large-area polymer solar cells. With the flow rate and the number of spray passes listed in Table 1, the devices with 1.0 cm^2 (square) and 10.2 cm^2 (12 mm × 85 mm) were fabricated, sample pictures, *J–V* curves of the devices, and the corresponding parameters are given in Fig. 6 and Table S5, respectively. From these data it can be seen that when the device area extends to 10 times (1.0 cm^2), the variation in efficiency agrees well with that with 9 mm^2, increasing from 3.7% to 4.6% with the improvement of short-circuit current and the fill factor. If the device area further increases to 100 times (10.2 cm^2), same trend still exists. Although the area expansion of the device brings a negative effect on efficiency due to the increase in intrinsic series resistance [60], for example, the PCE decreases from 5.1% (9 mm^2) to 4.1%, the advantages of this strategy such as simplicity without additional treatment steps, easy operating, cost-effectiveness, and the positive possibility of the application for other techniques in terms of the principle make it promising for the continuous fabrication of large-area polymer solar cells.

4. Conclusion

In summary, the present work provides an effective method, which involves only the fine manipulation of operation parameters, to construct desirable vertical morphology for spray-coated PBDT-TFQ/$PC_{71}BM$ blend films. With decreasing the ink flow rate (increasing the number of spray passes), more obvious enrichment of the PBDT-TFQ and $PC_{71}BM$ components takes place near the anode and cathode surfaces, respectively, which is associated with the solvent evaporation, the surface property of solution, the interaction with PEDOT:PSS, and the processing additive DIO. This vertical phase separation is beneficial for the efficient charge transportation as well as eventual charge collection, and thus improves the device efficiency. Based on this approach, the devices with the areas of 1.0 and 10.2 cm^2 reach efficiencies of 4.6% and 4.1%, respectively, which are, to the best of our knowledge, the highest values for the PSCs with identical areas fabricated by spray-coating technique under ambient atmosphere. The method proposed in this study is simple with no additional treatment steps, easy to operate, cost-effective, and suitable for other techniques, and thus shows great promise for fabricating large-area polymer solar cells.

Acknowledgements

This work was supported by the National Natural Science Foundation of China (Grant No. 20990233), Hi-Tech Research and Development Program (863) of China (Grant No. 2011AA050524), Solar Energy Initiative (KGCX2-YW-399 +9) of the Chinese Academy of Sciences. X.Y. would also like to thank the Fund for Distinguished Young Scholars (20925415) of NSFC.

Appendix A. Supplementary data

Supplementary data associated with this article can be found, in the online version, at http://dx.doi.org/10.1016/j.orgel.2015.07.010.

References

[1] G. Li, R. Zhu, Y. Yang, Polymer solar cells, Nat. Photon. 6 (2012) 153–161.
[2] F.C. Krebs, Fabrication and processing of polymer solar cells: a review of printing and coating techniques, Sol. Energy Mater. Sol. Cells 93 (2009) 394–412.
[3] Z.C. He, C.M. Zhong, S.J. Su, M. Xu, H.B. Wu, Y. Cao, Enhanced power-conversion efficiency in polymer solar cells using an inverted device structure, Nat. Photon. 6 (2012) 591–595.
[4] J.J. van Franeker, D. Westhoff, M. Turbiez, M.M. Wienk, V. Schmidt, R.A.J. Janssen, Controlling the dominant length scale of liquid–liquid phase separation in spin-coated organic semiconductor films, Adv. Funct. Mater. 25 (2015) 855–863.
[5] C. Gu, Y.C. Chen, Z.B. Zhang, S.F. Xue, S.H. Sun, C.M. Zhong, H.H. Zhang, Y. Lv, F.H. Li, F. Huang, Y.G. Ma, Achieving high efficiency of PTB7-based polymer solar cells via integrated optimization of both anode and cathode interlayers, Adv. Energy Mater. 4 (2014) 1301771.
[6] M. Campoy-Quiles, T. Ferenczi, T. Agostinelli, P.G. Etchegoin, Y. Kim, T.D. Anthopoulos, P.N. Stavrinou, D.D.C. Bradley, J. Nelson, Morphology evolution via self-organization and lateral and vertical diffusion in polymer: fullerene solar cell blends, Nat. Mater. 7 (2008) 158–164.
[7] X.N. Yang, J. Loos, S.C. Veenstra, W.J.H. Verhees, M.M. Wienk, J.M. Kroon, M.A.J. Michels, R.A.J. Janssen, Nanoscale morphology of high-performance polymer solar cells, Nano Lett. 5 (2005) 579–583.
[8] G. Li, V. Shrotriya, J.S. Huang, Y. Yao, T. Moriarty, K. Emery, Y. Yang, High-efficiency solution processable polymer photovoltaic cells by self-organization of polymer blends, Nat. Mater. 4 (2005) 864–868.
[9] Y.M. Sun, G.C. Welch, W.L. Leong, C.J. Takacs, G.C. Bazan, A.J. Heeger, Solution-processed small-molecule solar cells with 6.7% efficiency, Nat. Mater. 11 (2012) 44–48.
[10] J. Peet, J.Y. Kim, N.E. Coates, W.L. Ma, D. Moses, A.J. Heeger, G.C. Bazan, Efficiency enhancement in low-bandgap polymer solar cells by processing with alkane dithiols, Nat. Mater. 6 (2007) 497–500.
[11] L. Ye, S.Q. Zhang, W.C. Zhao, H.F. Yao, J.H. Hou, Highly efficient 2D-conjugated benzodithiophene-based photovoltaic polymer with linear alkylthio side chain, Chem. Mater. 26 (2014) 3603–3605.
[12] K.H. Hendriks, G.H.L. Heintges, V.S. Gevaerts, M.M. Wienk, R.A.J. Janssen, High-molecular-weight regular alternating diketopyrrolopyrrole-based terpolymers for efficient organic solar cells, Angew. Chem., Int. Ed. 52 (2013) 8341–8344.
[13] Z.B. Henson, G.C. Welch, T. van der Poll, G.C. Bazan, Pyridalthiadiazole-based narrow band gap chromophores, J. Am. Chem. Soc. 134 (2012) 3766–3779.
[14] A.B. Yusoff, D. Kim, H.P. Kim, F.K. Shneider, W.J. da Silva, J. Jang, A high efficiency solution processed polymer inverted triple-junction solar cell exhibiting a power conversion efficiency of 11.83%, Energy Environ. Sci. 8 (2015) 303–316.
[15] J. You, L. Dou, K. Yoshimura, T. Kato, K. Ohya, T. Moriarty, K. Emery, C.C. Chen, J. Gao, G. Li, Y. Yang, A polymer tandem solar cell with 10.6% power conversion efficiency, Nat. Commun. 4 (2013) 1446.
[16] Y.Y. Liang, Z. Xu, J.B. Xia, S.T. Tsai, Y. Wu, G. Li, C. Ray, L.P. Yu, For the bright future-bulk heterojunction polymer solar cells with power conversion efficiency of 7.4%, Adv. Mater. 22 (2010) E135–E138.
[17] Z. Xiao, Y. Yuan, B. Yang, J. VanDerslice, J. Chen, O. Dyck, G. Duscher, J. Huang, Universal formation of compositionally graded bulk heterojunction for

efficiency enhancement in organic photovoltaics, Adv. Mater. 26 (2014) 3068–3075.
[18] X. Guo, M.J. Zhang, W. Ma, L. Ye, S.Q. Zhang, S.J. Liu, H. Ade, F. Huang, J.H. Hou, Enhanced photovoltaic performance by modulating surface composition in bulk heterojunction polymer solar cells based on PBDTTT-C-T/PC71BM, Adv. Mater. 26 (2014) 4043–4049.
[19] T. Wang, N.W. Scarratt, H. Yi, A.D.F. Dunbar, A.J. Pearson, D.C. Watters, T.S. Glen, A.C. Brook, J. Kingsley, A.R. Buckley, M.W.A. Skoda, A.M. Donald, R.A.L. Jones, A. Iraqi, D.G. Lidzey, Fabricating high performance, donor–acceptor copolymer solar cells by spray-coating in air, Adv. Energy Mater. 3 (2013) 505–512.
[20] X.G. Guo, N.J. Zhou, S.J. Lou, J. Smith, D.B. Tice, J.W. Hennek, R.P. Ortiz, J.T.L. Navarrete, S.Y. Li, J. Strzalka, L.X. Chen, R.P.H. Chang, A. Facchetti, T.J. Marks, Polymer solar cells with enhanced fill factors, Nat. Photon. 7 (2013) 825–833.
[21] H.Y. Lv, X.L. Zhao, W.T. Xu, H. Li, J.Y. Chen, X.N. Yang, Improving performance of polymer solar cells based on PSBTBT/PC71BM via controlled solvent vapor annealing, Org. Electron. 14 (2013) 1874–1881.
[22] H. Li, H.W. Tang, L.G. Li, W.T. Xu, X.L. Zhao, X.N. Yang, Solvent-soaking treatment induced morphology evolution in P3HT/PCBM composite films, J. Mater. Chem. 21 (2011) 6563–6568.
[23] L. Ye, Y. Jing, X. Guo, H. Sun, S.Q. Zhang, M.J. Zhang, L.J. Huo, J.H. Hou, Remove the residual additives toward enhanced efficiency with higher reproducibility in polymer solar cells, J. Phys. Chem. C 117 (2013) 14920–14928.
[24] C.N. Hoth, S.A. Choulis, P. Schilinsky, C.J. Brabec, High photovoltaic performance of inkjet printed polymer: Fullerene blends, Adv. Mater. 19 (2007) 3973–3978.
[25] D. Angmo, T.T. Larsen-Olsen, M. Jorgensen, R.R. Sondergaard, F.C. Krebs, Roll-to-roll inkjet printing and photonic sintering of electrodes for ITO free polymer solar cell modules and facile product integration, Adv. Energy Mater. 3 (2013) 172–175.
[26] P. Kubis, L. Lucera, F. Machui, G. Spyropoulos, J. Cordero, A. Frey, J. Kaschta, M.M. Voigt, G.J. Matt, E. Zeira, C.J. Brabec, High precision processing of flexible P3HT/PCBM modules with geometric fill factor over 95%, Org. Electron. 15 (2014) 2256–2263.
[27] F. Machui, L. Lucera, G.D. Spyropoulos, J. Cordero, A.S. Ali, P. Kubis, T. Ameri, M.M. Voigt, C.J. Brabec, Large area slot-die coated organic solar cells on flexible substrates with non-halogenated solution formulations, Sol. Energy Mater. Sol. Cells 128 (2014) 441–446.
[28] S.E. Shaheen, R. Radspinner, N. Peyghambarian, G.E. Jabbour, Fabrication of bulk heterojunction plastic solar cells by screen printing, Appl. Phys. Lett. 79 (2001) 2996–2998.
[29] P. Sommer-Larsen, M. Jorgensen, R.R. Sondergaard, M. Hosel, F.C. Krebs, It is all in the pattern-high-efficiency power extraction from polymer solar cells through high-voltage serial connection, Energy Technol.-Ger. 1 (2013) 15–19.
[30] F.D. Yan, J. Noble, J. Peltola, S. Wicks, S. Balasubramanian, Semitransparent OPV modules pass environmental chamber test requirements, Sol. Energy Mater. Sol. Cells 114 (2013) 214–218.
[31] P. Schilinsky, C. Waldauf, C.J. Brabec, Performance analysis of printed bulk heterojunction solar cells, Adv. Funct. Mater. 16 (2006) 1669–1672.
[32] P. Kopola, T. Aernouts, S. Guillerez, H. Jin, M. Tuomikoski, A. Maaninen, J. Hast, High efficient plastic solar cells fabricated with a high-throughput gravure printing method, Sol. Energy Mater. Sol. Cells 94 (2010) 1673–1680.
[33] P. Kopola, T. Aernouts, R. Sliz, S. Guillerez, M. Ylikunnari, D. Cheyns, M. Valimaki, M. Tuomikoski, J. Hast, G. Jabbour, R. Myllyla, A. Maaninen, Gravure printed flexible organic photovoltaic modules, Sol. Energy Mater. Sol. Cells 95 (2011) 1344–1347.
[34] J.L. Yang, D. Vak, N. Clark, J. Subbiah, W.W.H. Wong, D.J. Jones, S.E. Watkins, G. Wilson, Organic photovoltaic modules fabricated by an industrial gravure printing proofer, Sol. Energy Mater. Sol. Cells 109 (2013) 47–55.
[35] K.X. Steirer, M.O. Reese, B.L. Rupert, N. Kopidakis, D.C. Olson, R.T. Collins, D.S. Ginley, Ultrasonic spray deposition for production of organic solar cells, Sol. Energy Mater. Sol. Cells 93 (2009) 447–453.
[36] D. Vak, S.-S. Kim, J. Jo, S.-H. Oh, S.-I. Na, J. Kim, D.-Y. Kim, Fabrication of organic bulk heterojunction solar cells by a spray deposition method for low-cost power generation, Appl. Phys. Lett. 91 (2007) 081102.
[37] J.G. Tait, C. Wong, D. Cheyns, M. Turbiez, B.P. Rand, P. Heremans, Ultrasonic spray coating of 6.5% efficient diketopyrrolopyrrole-based organic photovoltaics, IEEE J. Photovolt. 4 (2014) 1538–1544.
[38] J.G. Tait, B.P. Rand, P. Heremans, Concurrently pumped ultrasonic spray coating for donor: acceptor and thickness optimization of organic solar cells, Org. Electron. 14 (2013) 1002–1008.
[39] I. Etxebarria, J.G. Tait, R. Gehlhaar, R. Pacios, D. Cheyns, Surface treatment patterning of organic photovoltaic films for low-cost modules, Org. Electron. 14 (2013) 430–435.
[40] S. Bose, S.S. Keller, T.S. Alstrom, A. Boisen, K. Almdal, Process optimization of ultrasonic spray coating of polymer films, Langmuir 29 (2013) 6911–6919.
[41] D.L.F. Luettich, F. Seidel, D.R.T. Zahn, H. Graaf, C. von Borczyskowski, Morphological characterization of spray-coated PCBM thin films, Eur.-J. Surf. Sci. Nanotechnol. 10 (2012) 538–541.
[42] C. Girotto, D. Moia, B.P. Rand, P. Heremans, High-performance organic solar cells with spray-coated hole-transport and active layers, Adv. Funct. Mater. 21 (2011) 64–72.
[43] K.X. Steirer, J.J. Berry, M.O. Reese, M.F.A.M. van Hest, A. Miedaner, M.W. Liberatore, R.T. Collins, D.S. Ginley, Ultrasonically sprayed and inkjet printed thin film electrodes for organic solar cells, Thin Solid Films 517 (2009) 2781–2786.
[44] A.T. Barrows, A.J. Pearson, C.K. Kwak, A.D.F. Dunbar, A.R. Buckley, D.G. Lidzey, Efficient planar heterojunction mixed-halide perovskite solar cells deposited via spray-deposition, Energy Environ. Sci. 7 (2014) 2944–2950.
[45] M.V. Herst, C.J. Curtis, A. Miedaner, J. Nekuda, P. Hersh, J. Leisch, D.S. Ginley, Spray deposition of high quality CuInSe2 and CdTe films, Conf. Rec. IEEE Photovolt. Spec. Conf. (2008) 1–4.
[46] H. Back, J. Kong, H. Kang, J. Kim, J.R. Kim, K. Lee, Flexible polymer solar cell modules with patterned vanadium suboxide layers deposited by an electro-spray printing method, Sol. Energy Mater. Sol. Cells 130 (2014) 555–560.
[47] L. La Notte, D. Mineo, G. Polino, G. Susanna, F. Brunetti, T.M. Brown, A. Di Carlo, A. Reale, Fabrication of fully-spray-processed organic photovoltaic modules by using an automated process in air, Energy Technol.-Ger. 1 (2013) 757–762.
[48] J. Griffin, A.J. Pearson, N.W. Scarratt, T. Wang, D.G. Lidzey, A.R. Buckley, Organic photovoltaic devices incorporating a molybdenum oxide hole-extraction layer deposited by spray-coating from an ammonium molybdate tetrahydrate precursor, Org. Electron. 15 (2014) 692–700.
[49] C.N. Hoth, R. Steim, P. Schilinsky, S.A. Choulis, S.F. Tedde, O. Hayden, C.J. Brabec, Topographical and morphological aspects of spray coated organic photovoltaics, Org. Electron. 10 (2009) 587–593.
[50] S. Besold, U. Hoyer, J. Bachmann, T. Swonke, P. Schilinsky, R. Steim, C.J. Brabec, Quantitative imaging of shunts in organic photovoltaic modules using lock-in thermography, Sol. Energy Mater. Sol. Cells 124 (2014) 133–137.
[51] S. Hong, M. Yi, H. Kang, J. Kong, W. Lee, J.R. Kim, K. Lee, Effect of solvent on large-area polymer-fullerene solar cells fabricated by a slot-die coating method, Sol. Energy Mater. Sol. Cells 126 (2014) 107–112.
[52] T.R. Andersen, H.F. Dam, M. Hosel, M. Helgesen, J.E. Carle, T.T. Larsen-Olsen, S.A. Gevorgyan, J.W. Andreasen, J. Adams, N. Li, F. Machui, G.D. Spyropoulos, T. Ameri, N. Lemaitre, M. Legros, A. Scheel, D. Gaiser, K. Kreul, S. Berny, O.R. Lozman, S. Nordman, M. Valimaki, M. Vilkman, R.R. Sondergaard, M. Jorgensen, C.J. Brabec, F.C. Krebs, Scalable, ambient atmosphere roll-to-roll manufacture of encapsulated large area, flexible organic tandem solar cell modules, Energy Environ. Sci. 7 (2014) 2925–2933.
[53] S.-Y. Park, Y.-J. Kang, S. Lee, D.-G. Kim, J.-K. Kim, J.H. Kim, J.-W. Kang, Spray-coated organic solar cells with large-area of 12.25cm2, Sol. Energy Mater. Sol. Cells 95 (2011) 852–855.
[54] W.X. Zhiyong Liu, Ning Wang, Xiaoniu Yang, Preparation of large area inverted polymer solar cells by spray coating technique, Chin. J. Appl. Chem. 29 (2012) 1423–1427.
[55] H.-C. Chen, Y.-H. Chen, C.-C. Liu, Y.-C. Chien, S.-W. Chou, P.-T. Chou, Prominent short-circuit currents of fluorinated quinoxaline-based copolymer solar cells with a power conversion efficiency of 8.0%, Chem. Mater. 24 (2012) 4766–4772.
[56] J.G. Tait, B.J. Worfolk, S.A. Maloney, T.C. Hauger, A.L. Elias, J.M. Buriak, K.D. Harris, Spray coated high-conductivity PEDOT:PSS transparent electrodes for stretchable and mechanically-robust organic solar cells, Sol. Energy Mater. Sol. Cells 110 (2013) 98–106.
[57] P.H. Wobkenberg, J. Ball, F.B. Kooistra, J.C. Hummelen, D.M. de Leeuw, D.D.C. Bradley, T.D. Anthopoulos, Low-voltage organic transistors based on solution processed semiconductors and self-assembled monolayer gate dielectrics, Appl. Phys. Lett. 93 (2008) 013303.
[58] S.J. Lou, J.M. Szarko, T. Xu, L.P. Yu, T.J. Marks, L.X. Chen, Effects of additives on the morphology of solution phase aggregates formed by active layer components of high-efficiency organic solar cells, J. Am. Chem. Soc. 133 (2011) 20661–20663.
[59] Y. Yao, J. Hou, Z. Xu, G. Li, Y. Yang, Effects of solvent mixtures on the nanoscale phase separation in polymer solar cells, Adv. Funct. Mater. 18 (2008) 1783–1789.
[60] D. Gupta, M. Bag, K.S. Narayan, Area dependent efficiency of organic solar cells, Appl. Phys. Lett. 93 (2008) 163301.